Buckling of Orthotropic Plates with One Free Edge

A. Holston Jr.*
Martin Marietta Corporation, Denver, Colo.

Nomenclature

a,b = length and width of plate; see Fig. 1
D_1 = $D_{11} = E_{xx}h^3/[12(1 - \nu_{xy}\nu_{yx})]$
D_2 = $D_{22} = E_{yy}h^3/[12(1 - \nu_{xy}\nu_{yx})]$
D_{12} = $\nu_{yx}D_1 = \nu_{xy}D_2$
D_{66} = $G_{xy}h^3/12$
D_3 = $D_{12} + 2D_{66}$
E_{xx},E_{yy} = Young's modulus in x and y directions, respectively
G_{xy} = shear modulus in x,y plane
h = plate thickness
m = number of half-waves of buckling displacement in x direction
N_{xx} = compressive stress resultant that causes buckling
w = transverse buckling displacement
α = E_{xx}/E_{yy}
β = ν_{xy}
γ = $2G_{xy}/E_{yy}$
ζ = b/a
ν_{xy},ν_{yx} = Poisson's ratios; first subscript denotes load direction, second subscript denotes transverse strain direction
σ = $N_{xx}b^2/(\pi^2m^2D_1)$
χ = $\{[\beta + \gamma(1 - \beta^2/\alpha)]^2 - \alpha + \alpha\sigma/\zeta^2\}^{1/2}$
ψ = $\gamma(1 - \beta^2/\alpha) + \beta$
ω = $\gamma(1 - \beta^2/\alpha)$

Introduction

THE high values of specific moduli and strengths of fiber-reinforced composite materials make them attractive for aerospace structural components such as beams, columns, and stiffeners. These members are frequently loaded in compression and they may fail by buckling as an "Euler Column" or by local buckling. The local buckling of the flanges and legs of these members is analogous to the buckling of a plate with one free edge and loaded uniformly parallel to the free edge.

A stability analysis of isotropic plates simply supported on three sides and free on the fourth side under uniform compression parallel to the free edge has been given by Timoshenko.[1] Experiments conducted by Bridget, Jerome, and Vosseller[2] on the compression of angles show good agreement with the theory of Ref. 1. Lackman and Ault[3] extended the analysis of Ref. 1 to orthotropic plates but their transcendental equation for buckling loads contains an error. Buckling load curves, based on the transcendental equation of Ref. 3, are shown in Ref. 4.

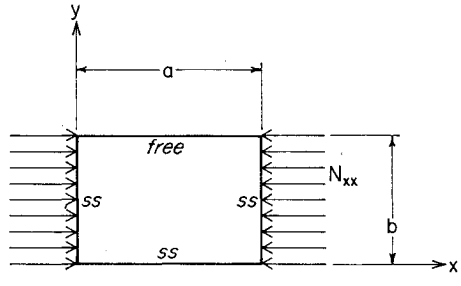

Fig. 1 Coordinate system.

Received December 17, 1969.
* Senior Research Scientist. Member AIAA.

This Note corrects the error of Ref. 3 and shows buckling load curves for boron-epoxy, carbon-epoxy, and fiberglass-epoxy plates. It also develops an approximate algebraic equation for the buckling load. Comparisons of approximate and exact buckling loads show that the maximum difference is less than 1%. This approximate equation shows optimum elastic properties and geometry.

Analysis and Results

The differential equation for the transverse buckling displacement of a homogeneous orthotropic thin plate whose principal elastic axes are coincident with the coordinate axes (Fig. 1) is

$$D_1w_{,xxxx} + 2D_3w_{,xxyy} + D_2w_{,yyyy} + N_{xx}w_{,xx} = 0 \quad (1)$$

In Ref. 3, the displacement field was taken as

$$w = f(y)\sin(\pi x/a) \quad (2)$$

The resulting stability equation of Ref. 3, Eq. (16), may be corrected by interchanging the subscripts of the first Poisson's ratio appearing in the definition of gamma used there. This correction may be verified from Eqs. (15) of Ref. 3. When this correction is made and a half-wave number "m" is introduced in the displacement field

$$w = f(y)\sin(m\pi x/a) \quad (3)$$

then the stability equation becomes

$$(\chi + \psi)^{1/2}(\chi - \omega)^{\frac{1}{2}}\tan[m\pi\zeta(\chi - \psi)^{1/2}] = (\chi - \psi)^{1/2}(\chi + \omega)^2\tanh[m\pi\zeta(\chi + \psi)^{1/2}] \quad (4)$$

In this equation ψ and ω depend upon elastic properties, ζ is the slenderness ratio, and χ contains the buckling load. This equation reduces to the equation given by Timoshenko[1] for isotropic materials.

A cursory examination of Eq. (4) shows that

$$\chi = \psi \quad (5)$$

is a solution. The buckling load given by this solution is

$$N_{xx} = D_1(m\pi/a)^2 \quad (6)$$

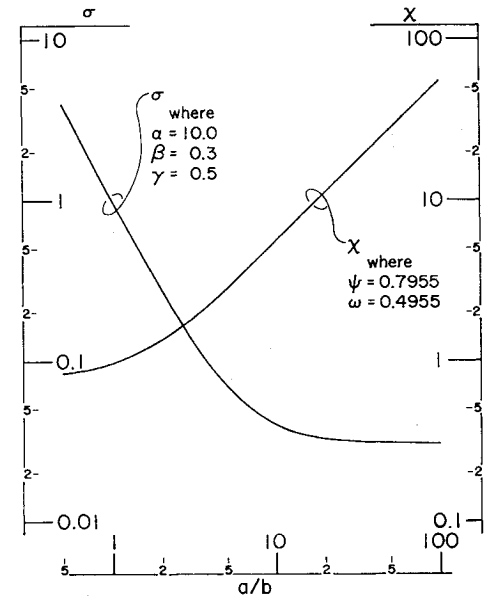

Fig. 2 Critical loads for boron-epoxy plates.

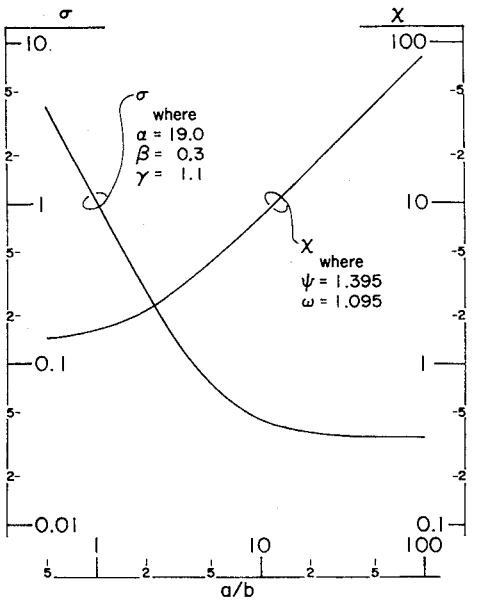

Fig. 3 Critical loads for carbon-epoxy plates.

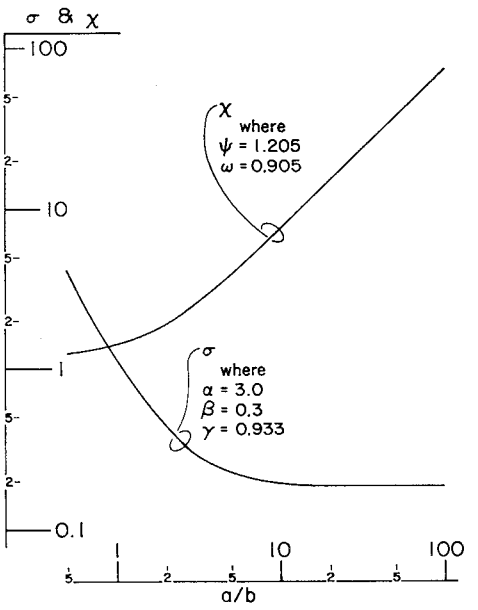

Fig. 4 Critical loads for fiberglass-epoxy plates.

References 1 and 3 restrict themselves to buckling loads greater than those given by Eq. (6) because of "constraints" along the sides $y = 0$ and $y = b$. Additional insight into the exclusion of the buckling load given by Eq. (6) follows.

The governing equation for $f(y)$ is obtained by substituting Eq. (3) into Eq. (1)

$$D_2 f^{IV}(y) - 2D_3(m\pi/a)^2 f^{II}(y) + (m\pi/a)^2[D_1(m\pi/a)^2 - N_{xx}]f(y) = 0 \quad (7)$$

The form of the solution for $f(y)$ depends upon the coefficient of $f(y)$ in Eq. (7). For $N_{xx} > D_1(m\pi/a)^2$ the general solution is

$$f(y) = C_1 \cosh[(m\pi y/a)(\chi + \psi)^{1/2}] + C_2 \sinh[(m\pi y/a)(\chi + \psi)^{1/2}] + C_3 \cos[(m\pi y/a)(\chi - \psi)^{1/2}] + C_4 \sin[(m\pi y/a)(\chi - \psi)^{1/2}] \quad (8)$$

which was used in Refs. 1 and 3. When $N_{xx} = D_1(m\pi/a)^2$ the general solution of Eq. (7) is

$$f(y) = C_1 y + C_2 + C_3 \cosh[(m\pi y/a)(2\psi)^{1/2}] + C_4 \sinh[(m\pi y/a)(2\psi)^{1/2}] \quad (9)$$

Substitution of Eq. (9) into the boundary condition equations shows that the following equation must be satisfied in order to obtain a nontrivial solution for the buckling displacement:

$$\tanh[(m\pi b/a)(2\psi)^{1/2}] = (m\pi b/a)(2\psi)^{1/2}(\psi - \omega)^2/(\psi - \omega)^2 \quad (10)$$

This equation shows that for given elastic parameters (ψ,ω) and wave number (m) there is a single value of slenderness ratio (b/a) for which the buckling displacement associated with the buckling load given by Eq. (6) is nontrivial. For isotropic materials, Eq. (10) reduces to

$$\tanh(2^{1/2}m\pi b/a) = 2^{1/2}(m\pi b/a)\nu^2/(2 - \nu)^2 \quad (11)$$

Setting $\tanh(2^{1/2}m\pi b/a) = 1$, since $\tanh Z \approx 1$ for large values of Z, in Eq. (11) gives

$$b/a = (2 - \nu)^2/(2^{1/2}m\pi\nu^2) \quad (12)$$

Evaluation of Eq. (12) with $\nu = \frac{1}{4}$ and $m = 1$ gives $b/a = 11$. Thus, the buckling load given by Eq. (6) is for a very short isotropic plate.

Another solution of Eq. (4) has been developed for $N_{xx} > D_1(m\pi a)^2$. It was obtained by iteration and reduces to the solution of Ref. 1 for isotropic materials. Figure 2 shows the variation of this solution (χ) and dimensionless buckling load (σ) with a/b for values of elastic parameters which are typical of boron-epoxy composites. Note that only two elastic parameters (ψ and ω) are required to define χ, but three parameters (α, β, and γ) are necessary for σ. Similar results are shown in Figs. 3 and 4 for carbon-epoxy and fiberglass-epoxy, respectively. These figures show that the buckling load is independent of a/b for large values of a/b. Calculations were made with half-wave number (m) equal to one, two, and three. The smallest buckling load was obtained with $m = 1$ in all cases and it is the value shown. Evaluation of Eq. (10) with $m = 1$ gives $b/a = 4.7$, 13, and 10 for the elastic properties shown in Figs. 2, 3, and 4, respectively. Hence, the buckling loads given by Eq. (6) are for very short orthotropic plates.

An approximate expression for the buckling load has been developed by the energy method. The potential energy of bending is[5]

$$\Delta V = \frac{1}{2}\int_0^a \int_0^b [D_{11}w_{,xx}^2 + 2D_{12}w_{,xx}w_{,yy} + D_{22}w_{,yy}^2 + 4D_{66}w_{,xy}^2]\,dxdy \quad (13)$$

and the work done by the external load is

$$\Delta U = \left(\frac{N_{xx}}{2}\right)\int_0^a \int_0^b w_{,x}^2 dxdy \quad (14)$$

The buckling displacement is taken as

$$w = c_1 y \sin(m\pi x/a) \quad (15)$$

which satisfies boundary conditions on the simply supported edges but does not satisfy the free edge condition. Substitution of Eq. (15) into the equation obtained by setting $\Delta U = \Delta V$ gives

$$\sigma = 6(1 - \beta^2/\alpha)\gamma/(\alpha m^2\pi^2) + \zeta^2 \quad (16)$$

which reduces to the expression given in Ref. 1 for isotropic materials with Poisson's ratio equal to $\frac{1}{4}$. The first term of this equation is independent of slenderness ratio (ζ) and it is the dominant term for long plates. For short plates the second term is dominant and it is the solution given by Eq. (5). Comparison of buckling loads given by Eq. (16) with those

obtained from the iterative solution of Eq. (4) shows that the maximum difference is less than 1% for the parameters shown in Figs 2–4. Equation (16) may be written in dimensional form as

$$N_{xx} = h^3\{G_{xy}/b^2 + m^2\pi^2E_{xx}/[12a^2(1 - \nu_{xy}^2E_{yy}/E_{xx})]\} \quad (17)$$

This equation shows that the smallest buckling load is obtained with $m = 1$. It also shows that the shear modulus (G_{xy}) is dominant for long plates and that the other properties become important for short plates.

References

[1] Timoshenko, S. and Gere, J. M., *Theory of Elastic Stability*, McGraw-Hill, New York, 1961, pp. 361–363.

[2] Bridget, F. J., Jerome, C. C., and Vosseller, A. B., "Some New Experiments on Buckling of Thin-Wall Construction," *Transactions of the ASME, Applied Mechanics Division*, Vol. 56, 1934, pp. 569–578.

[3] Lackman, L. M. and Ault, R. M., "Minimum-Weight Analysis of Filamentary Composite Wide Columns," *Journal of Aircraft*, Vol. 5, No. 2, March–April 1968, pp. 184–190.

[4] "Advanced Composite Wing Structures; Preliminary Analysis and Optimization Methods," Tech. Rept. AC-SM-7843, Aug. 1968, Grumman Aircraft Engineering Corporation.

[5] Lekhnitski, S. G., *Anisotropic Plates*, 2nd ed., OGIZ, Moscow-Leningrad, 1947; English ed. translated by S. W. Tsai and T. Cheron, Gordon and Breach, London, 1968.

Equilibrium Shape of an Ablating Nose in Laminar Hypersonic Flow

F. D. Hains*

The Aerospace Corporation, El Segundo, Calif.

During re-entry, the nose of a body may change shape as ablation occurs. In a series of experiments with teflon models, Simpkins[1] obtained stable shapes that were independent of the initial shape of the nose. He also developed a simple theory that gave a final shape not in good agreement with his experimental results. This Note presents a new theory for the equilibrium shape associated with a laminar boundary layer. Numerical results from the theory are then compared with some recent experimental shapes obtained in the Aerospace Corp. arc tunnel. A similar study of the equilibrium shape for a wholly turbulent boundary layer was made by Welsh.[2]

Consider a circular cylinder with a nose that is undergoing ablation and has reached a stable shape. The local rate of surface erosion is assumed to be proportional to q, the local rate of heat transfer into the body surface. For a stable shape, the condition for uniform axial erosion is

$$q/q_0 = \cos\alpha \quad (1)$$

where α is the angle between the normal to the body surface and the body axis, and q_0 is the stagnation point heat transfer.

Simpkins used the local heat transfer expression

$$Nu/(Re)^{1/2} = 0.66 \quad (2)$$

which is applicable only in the vicinity of the stagnation point. The Nusselt number and Reynolds number are, respectively, for unit Prandtl number

$$Nu = qS/\nu_w(H_1 - h_w) \quad (3)$$

$$Re = U_1S/\nu_w \quad (4)$$

where S is the distance along the body measured from the nose, H_1 and U_1 are the total enthalpy and velocity, respectively, at the outer edge of the boundary layer, and h_w and ν_w are the wall values of enthalpy and kinetic viscosity, respectively. Simpkins approximated the velocity by $U_1 = S(dU_1/dS)_0$, where the derivative is evaluated at the stagnation point. With this assumption, $Re \sim S^2$ and a cancellation with the S in Eq. (3) leaves Eq. (2) independent of a length scale. As a result, Simpkins predicts an equilibrium nose shape whose size is specified by freestream conditions. This is unrealistic because the nose shape should depend on the body scale as well as freestream conditions.

The lack of a body scale was overcome in the present analysis by replacing Eq. (2) with a better estimate of the local heat-transfer rate. The heat-transfer relation for blunt bodies given by Lees[3] is

$$q/q_0 = yfT/\left[2\left(\int_0^S y^2f ds\right)^{1/2}\right] \quad (5)$$

where

$$f = (p_1/p_0)(U_1/U_\infty) \quad (6)$$

$$T = (U_\infty R_0/\beta_0)^{1/2} \quad (7)$$

Here, p_0 is the stagnation pressure behind the bow shock, U_∞ is the freestream velocity, $\beta_0 = (dU_1/d\alpha)_0$ evaluated at the stagnation point, and R_0 is the nose radius. The quantities p_1 and U_1 are the values of pressure and velocity, respectively, evaluated at the outer edge of the boundary, y is the distance from a point on the body surface to the body axis, and S is the distance to the stagnation point along the body surface.

From the geometry of the body surface

$$ds = dy/\cos\alpha \quad (8)$$

and

$$dx = dy\tan\alpha \quad (9)$$

where x is the coordinate along the centerline of the body. Substituting Eqs. (1) and (8) into Eq. (5), we get

$$\frac{y}{a} = \frac{2\cos\alpha}{fT^3}\left(\frac{T^2}{R_0}\right)\left(\frac{R_0}{a}\right)\left(\int_0^y \frac{y^2f}{\cos\alpha}\,dy\right)^{1/2} \quad (10)$$

which is satisfied by

$$(y/a) = (R_0/a)(T^2/R_0)(f/\cos\alpha) \quad (11)$$

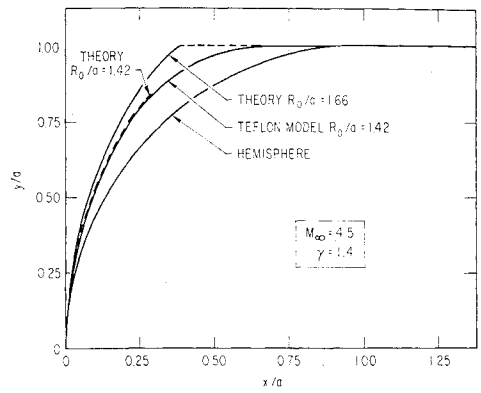

Fig. 1 Comparison of theoretical shapes with experimental shape.

Received December 19, 1969; revision received March 16, 1970. This work was supported by the U.S. Air Force under Contract F04701-69-C-0066.

* Member of the Technical Staff, Aerodynamics and Heat Transfer Department, Aerodynamics and Propulsion Research Laboratory; presently at Bell Aerospace Co., Buffalo, N. Y.